Editor's Note: The following four articles show the possibilities that computer-assisted tomography (CAT) and magnetic resonance imaging (MRI) provide to understanding structure, permeability and fluid distribution in porous media, with applications to oil and natural gas production, fluidized and trickle beds, and related processes. Advanced imaging methods are beginning to produce useful 2-D and 3-D views of geometrically complex phenomena in real time. These research articles on CAT and MRI applied to problems involving porous solids were presented in a session at the April 1993 National AIChE meeting in Houston, organized by A. Kantzas. They went through regular *Journal* selection procedures and survived the demanding *Journal* review process.

Determining Fluid Saturations during Multiphase Flow Experiments by NMR Imaging Techniques

Songhua Chen, Fangfang Qin, and A. Ted Watson
Dept. of Chemical Engineering, Texas A&M University, College Station, TX 77843

The quantitative determination of porosity and saturation distributions in porous media using unclear magnetic resonance imaging techniques is addressed. A method based on multiple image acquisitions with extrapolation within a model of transverse relaxation was investigated for new experimental situations. The determination of saturation was validated with limestone and sandstone samples. Experimental evidence for dependencies of transverse relaxation and linewidth on saturation is discussed, as well as their impact on image resolution and quantitation. An automatic production measurement device for independent verification of average saturations during dynamic experiments is investigated.

Introduction

Quantitative determination of fluid saturation distributions is a fundamental measurement to characterize fluid storage and transport in multiphase processes in porous media. Conventional methods provide measures of fluid quantities only as bulk or average properties. In contrast, NMR imaging techniques can provide unprecedented information about fluid-phase distributions in porous media during displacement processes and can be used to distinguish fluid phases in systems where multiple fluid phases are involved.

Spin density imaging methods can be used to determine information concerning porosity and saturation distributions (Edelstein et al., 1988; Baldwin and Yamanashi, 1986; Mandava et al., 1990; Chen et al., 1992, 1993). Accurate quantitation of these data is difficult because of the characteristically short relaxation times of fluids in porous media and because of variation of relaxation properties with position and saturation. Chen et al. (1992; 1993) have developed a general approach for determination of porosity and saturation distributions in porous media from NMR spin-density images. The approach is based on multiecho acquisitions with multicomponent relaxation models for estimation of the intrinsic spin density. The method was validated by comparing averages of porosity distributions obtained by NMR imaging with average porosities determined gravimetrically. A validation under conditions for which the sample contains two fluid phases has not been reported.

Further validation of this method for multiphase situations is desired due to some difficulties which arise in multiphase and dynamic situations. We have observed that NMR relaxation times and spectral linewidths of fluids in porous media are saturation-dependent. The effect of transverse relaxation on image acquisition has been reported by Chen et al. (1992), but information regarding effects of saturation on linewidth has not been reported. In this article, experimental evidence of saturation dependent linewidth is reported for a sandstone sample, and its impact on image resolution is discussed.

Another consideration is the utility of the developed procedures for samples with very short transverse relaxation times. Due to equipment limitations, significant relaxation occurs before acquisition of the spin-echo signal. Previous applications of the method have been with relatively clean outcrop samples. In this work, the procedures are tested with a core

sample from a producing reservoir which has a considerably shorter transverse relaxation time than previous samples, thus providing a more stringent test for the method.

Two types of experiments were conducted to evaluate the procedures for quantitative determination of fluid saturations. First, saturations were determined under static conditions for an air-water system in a limestone sample. The method was validated by comparing the averages of the saturation distributions determined by NMR imaging with those obtained gravimetrically. Second, averages of profile images measured during displacement experiments were compared with values determined by material balance. For this purpose, an automated measurement device was constructed to monitor the production of the displaced phase continuously throughout the dynamic displacement experiment. Air and water phases were separated by the large differences in their dielectric properties. This production device is inexpensive and easy to operate, yet reliable and sensitive to changes in fluid quantity.

Experimental Details

NMR Imaging Procedures

All NMR measurements were conducted with a GE 2-Tesla CSI-II imager/spectrometer with 31 cm magnet bore and equipped with a 20 G/cm shielded gradient coil and a birdcage RF coil. A modified version of the spin-echo FT imaging pulse sequence described by Chen et al. (1992) was used for acquiring multiecho longitudinal profile images. Multiple echoes with up to 22 different *TE* values were used to acquire profiles for each data set. The delay time $TR > 5T_1$ was used so that the effects of T_1 relaxation were eliminated. For dynamic displacement experiments, a random order of the echo times was used to reduce the systematic errors. This profile imaging technique provides for rapid acquisition at large S/N (signal-to-noise), thus reducing flow artifacts during the dynamic displacement experiments.

Samples and experimental procedures

Four rock samples were prepared in cylindrical shape with 2.54 cm diameter: two Bentheimer sandstone samples and one Texas Cream limestone are cleaned outcrop cores, and the fourth sample is a reservoir sandstone from west Texas. For experiments involving two liquid phases, D_2O was used as the wetting phase and *n*-hexadecane was used as the nonwetting phase. The NMR probe was tuned to the proton frequency, and thus only the oleic phase was imaged.

Two different Bentheimer sandstone samples were used for the observation of saturation-dependent transverse relaxation times and linewidths. The experiments were conducted as drainage processes involving gas (N_2) and liquid (water) phases. Initially the samples were saturated with water and desaturated with pressurized N_2. For core 1, the process was stopped before the equilibrium state was reached, and profile image data were acquired for analyzing saturation and transverse relaxation distributions. For core 2, consecutive equilibrium partial saturation states were reached at which linewidths of the wetting-phase signal were measured. These equilibrium partial saturation states were obtained using a desaturation device (Chen et al., 1993).

The Texas Cream limestone sample was used in a series of experiments. The sample was first saturated with water and then desaturated to various partial water saturation states using a centrifuge. NMR profile images were acquired at these saturation states, and gravimetric measurements were used to obtain the overall saturation values.

The reservoir sample was cleaned using solvent agents (a mixture of chloroform and methanol) in an extractor for several days to remove hydrocarbons. Upon cleaning it was mounted in a Plexiglas core holder (Chen et al., 1992) and resaturated in the same way as for the Texas Cream limestone with pure *n*-hexadecane using an injection method. An imbibition experiment was conducted with this rock; images and production data were acquired during the displacement experiments.

Quantitative NMR Imaging for Fluid Distributions in Porous Media

The method for quantitative determination of porosity and saturation distributions in porous media using NMR image data has been developed by Chen et al. (1992). In that approach, multiple image acquisitions at different echo times (*TE*) are used and an extrapolation technique is employed to obtain the intrinsic magnetization. This intrinsic magnetization is proportional to the amount of the observed nuclei. In the frequency domain, it is related to the proton linear density in the sample, $N(z)$, by:

$$M_0(\omega) = k(z)N(z)\Delta z/\Delta\omega. \tag{1}$$

The pixel size Δz is subject to the strength of the readout gradient since $\omega = \gamma Gz$. Typically, pixel sizes of the order of 10^{-1} to 10^{0} mm can be achieved. The proportionality factor $k(z)$ can be determined using a reference standard included in the imaged volume (Mandava et al., 1990; Chen et al., 1992). The saturation distribution can then be obtained by forming the ratio between the values of the linear density obtained at any time with those obtained when the sample is fully saturated.

Due to the pore size variations over a core sample, it is often observed that the relaxation decay function varies from pixel to pixel and is not well represented by a single exponential. Consequently, the extrapolation procedures are best carried out on a pixel-by-pixel basis. A general multiexponential function may be used for modeling the relaxation decay:

$$M(\omega_i, TE) = \sum_{j=1}^{N_c} M_{0j}(\omega_i)\exp(-TE/T_{2ij}). \tag{2}$$

Values of N_c of 1, 2 and 3 would correspond to single, bi- and triexponential decays, respectively. Estimates for the intrinsic magnetization and the transverse relaxation parameters are obtained using nonlinear regression whereby the sum of squared differences between the observed and calculated values of magnetization is minimized. The number of terms N_c for the multiexponential model can be selected according to statistical criteria, such as the *F*-test:

$$F = \frac{[RSS(N_c - 1) - RSS(N_c)]/p}{RSS(N_c)/(n-m)}, \tag{3}$$

where n is the number of observed data, $m = 2N_c$, and $p =$

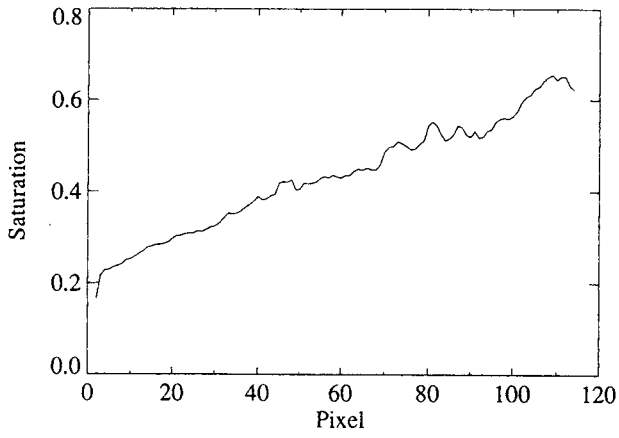

Figure 1. Saturation profile for Bentheimer core 1.

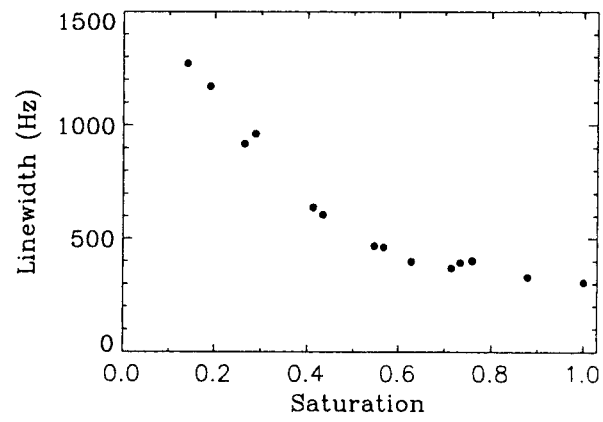

Figure 3. Saturation dependence of NMR spectral linewidth in Bentheimer core 2.

2 is the difference between the number of components in the simplified and more complete models.

This approach has been validated for porosity calculations in a number of different core samples (Chen et al., 1992, 1993). It has been found that the volume-averaged porosities calculated from NMR image data match satisfactorily with the average porosities obtained using gravimetric methods. Although it is straightforward to extend the same approach to dynamic experiments (Mandava et al, 1990; Chen et al., 1992, 1993) for estimation of saturation distributions, the accuracy of such estimates has not been verified. Independent measurements are desired since there are several experimental conditions associated with dynamic experiments and low saturations which could compromise the accuracy of saturation determination.

Effects of Saturation-Dependent Relaxation and Spectral Linewidth on Quantitative Images

It has been observed that the transverse relaxation time in porous media decreases as the saturation is lowered (Chen et al., 1992). Figure 1 shows the saturation profiles obtained for Bentheimer core 1. As mentioned in the section on Experimental Details, we prepared this sample with a nonequilibrium saturation distribution for the observation of saturation-dependent transverse relaxation. The T_2 relaxation parameters were analyzed pixel-by-pixel with a single exponential model, and the corresponding saturation values of individual pixels were recorded. The T_2-saturation profile is plotted in Figure 2. A significant variation in T_2 with saturation is observed. Since NMR images are acquired at finite echo times (TE), shorter T_2 values at low saturations could result in a significant decay of signal before images are acquired. This could become severe in cases where there is a very short T_2 component, since the contribution of this short component could decay completely before the signal is acquired.

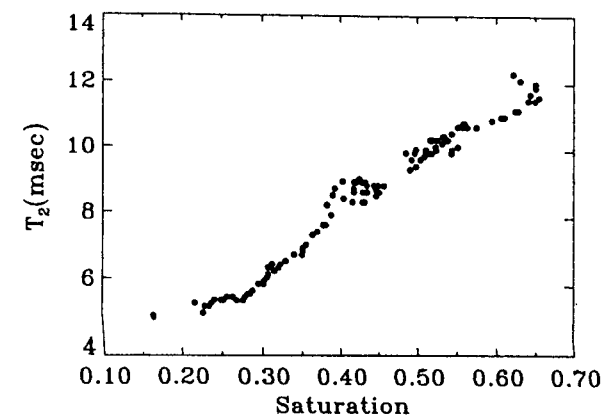

Figure 2. Saturation dependence of T_2 in Bentheimer core 1.

It is also observed that the NMR spectral linewidth is saturation-dependent. Figure 3 shows the NMR linewidth as a function of saturation in Bentheimer core 2. Since it is difficult to determine accurately the spectral width corresponding to each pixel in the presence of the applied magnetic gradient required for images, we studied the linewidth of the bulk sample at individual equilibrium saturation states using this relatively clean and homogeneous core sample. The linewidth was calculated from the NMR spectra fitted with Lorentzian line model. It is known that the inhomogeneous linebroadening in porous rocks can arise from the variations of magnetic susceptibility of the rock materials over the entire sample. The saturation dependence of the linewidth can be attributed to the fact that at low saturations a great proportion of the water molecules resides near the fluid-pore matrix interfacial regions, and thus that fluid phase is more vulnerable to the susceptibility variations occurring on the solid surfaces. In addition, the increased air-water interfacial area at lower water saturations provides additional susceptibility differences which may also contribute to linebroadening as the wetting-phase saturation is lowered.

An important effect of linewidth variation on image acquisition is the determination of susceptibility-limited image resolution. For systems with narrow NMR linewidths and a sufficiently strong magnetic field gradient, the pixel size

$$\Delta z = \frac{2\pi \Delta \nu_p}{\gamma G} \tag{4}$$

is equal to the image resolution, where $\Delta \nu_p$ is the frequency interval corresponding to individual pixel. Other effects, however, can also reduce the image resolution (Callaghan, 1991). In porous media, the most commonly encountered problem is

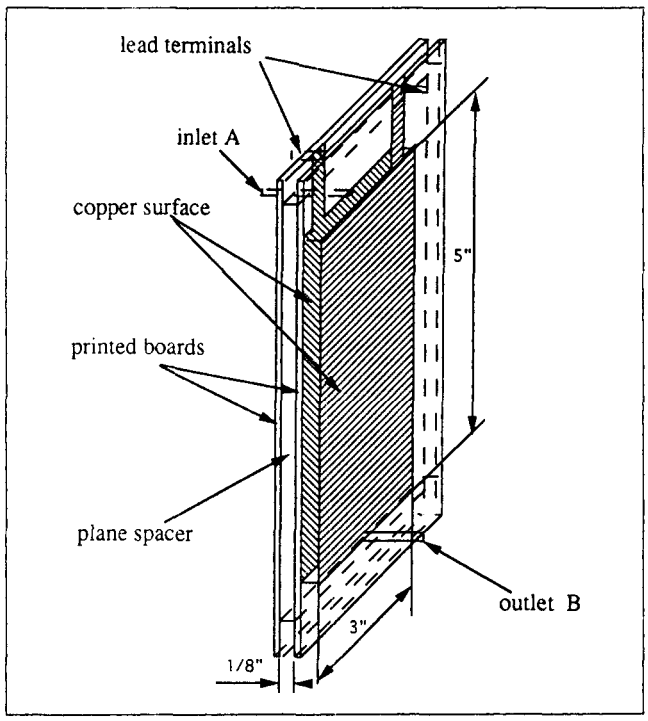

Figure 4. Capacitance device used for production measurements.

the susceptibility-limited (linewidth-limited) resolution. If the linewidth of a sample within a pixel, $\Delta\nu$, surpasses the pixel size $\Delta\nu_p$, the actual resolution in such cases should be calculated according to the linewidth, instead of $\Delta\nu_p$:

$$\Delta z_l = \frac{2\pi\Delta\nu}{\gamma G}. \tag{5}$$

Therefore, even though the pixel size has not changed, the actual image resolution is larger than a pixel size, resulting in overlapping of signals between adjacent pixels.

Figure 3 shows that the linewidths at very low saturations are several times greater than those at high saturations. Therefore, the actual image resolution corresponding to low-saturation states may not be the same as that for the fully-saturated state, if the linewidths $\Delta\nu$ at low saturations are greater than $\Delta\nu_p$. This could be a problem for displacement experiments which exhibit a range of saturations.

Equation 4 shows that for a fixed pixel size Δz increasing the strength of the applied gradient G could increase the frequency ranges covered by each pixel, $\Delta\nu_p$, to a limit determined by the allowable total spectral width, $n\nu_p$, of the imaging apparatus. Within this limit, it is desired to use a stronger gradient so that $\Delta\nu_p > \Delta\nu$ is valid for all saturations.

Production Measurements Using a Capacitance Device

Since a number of factors may affect image quantitation, it is desirable to have an independent means of verifying the saturations obtained by the imaging method. Under steady-state situations involving liquid and gas phases, such verification could be accomplished by comparing liquid-phase saturations obtained using both imaging and gravimetric methods. Other means are required for monitoring dynamic situations. Here we report a method for continuous measurement of production of one of the liquid phases. The average saturation is then determined through a material balance.

Determination of the amount of production of either fluid phase can be accomplished through a continuous measurement provided that there is a sufficient contrast between the properties of the fluid phases. Differences between the density (Kerig, 1985; Hvollboll, 1978), electrical (Weinbrandt et al., 1985) and optical (Sufi et al., 1982; Potter et al., 1989) properties have been used. We have developed an automated production measuring system which utilizes the large difference of dielectric constants between oil and water. Dielectric differences involving air/water phases have been used to monitor production *rates* by measuring frequencies with which oil and water pass through a capillary tube (Weinbrandt et al., 1985). In our device, the cumulative production of the displaced-phase fluid is measured. This should provide a much more accurate estimate of average saturation, which is desired for our purposes, than would integration of the production rate.

The device is shown in Figure 4. A parallel-plates-type capacitor design was used in which the volume between the plates serves as the container for the produced fluid. Capacitance is measured using a GLC1659 RLC Digibridger and is interfaced with an IBM PC for continuous sampling operation during displacement experiments. The container is initially filled with water before the displacement starts. The capacitance corresponding to the water-filled device is:

$$C_0 = \frac{\epsilon_w A}{d}, \tag{6}$$

where ϵ_w is the dielectric constant of water, $A = lw$ is the surface area of the plate, and d is the distance between the parallel plates. As the displacement experiment begins, fluid enters the top (position A), while excess fluid is drained from the bottom (B). A tube attached to the opening B is raised above the level of position A to keep the collection device filled. Since the oil is lighter than water, it will fill the upper portion of the capacitor volume while the water will fill the lower part. As displacement proceeds, the capacitance changes according to

$$C' = \frac{\epsilon_w A_1}{d} + \frac{\epsilon_o A_2}{d}, \tag{7}$$

where ϵ_o is the dielectric coefficient of oil, $A_1 = l_1 w = (l - l_2)w$ is the surface area of plate contacted by water in the capacitor volume and $A_2 = l_2 w$ is the surface area of plate contacted by oil. By subtracting Eq. 6 from Eq. 7, one obtains:

$$C = C' - C_0 = \frac{l_2 w(\epsilon_o - \epsilon_w)}{d}. \tag{8}$$

This indicates that C is linear with respect to the oil quantity ($\propto l_2 w$). In practice, a calibration was performed before the displacement experiments using D_2O and the same type of oil which was used for saturating the rocks. The calibration curve is shown in Figure 5. With the calibration, knowledge of the

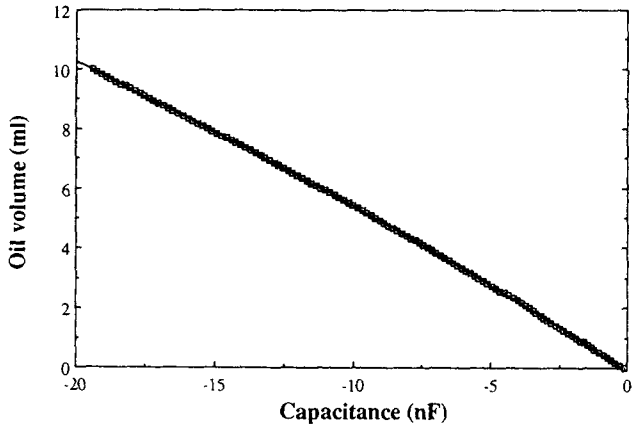

Figure 5. Capacitance calibration curve.

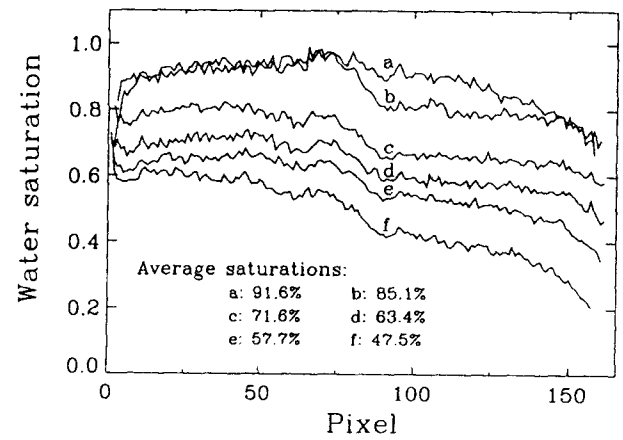

Figure 6. Saturation profiles corresponding to various partial saturation states in Texas Cream limestone.

dielectric constants of the fluids involved is unnecessary. Other types of liquids can also be used in this device simply by performing new calibrations.

A particular advantage of this design is the sensitivity of the measurements. By filling the capacitor with D_2O initially and letting oil displace D_2O, we are taking advantage of the large dielectric constant value of water (D_2O) in detecting the oil volume change. This can be easily understood from Eq. 8 where the change in the total capacitance C is proportional to $\epsilon_o - \epsilon_w$. Using this design, the change in the total capacitance corresponding to an oil volume increase, $\Delta V = \Delta l_2 wd$, is $\Delta C_1 \propto \Delta l_2(\epsilon_o - \epsilon_w)$. In contrast, if we let the production liquids fill in an empty container, the capacitance change for the same amount of oil increase will only be $\Delta C_2 \propto \Delta l_2 \epsilon_o$. Since $\epsilon_o \ll \epsilon_w$, the absolute value of ΔC_1 is much larger than the absolute value of ΔC_2. Therefore, it indicates that our design can improve sensitivity substantially. With the present design of $d = 0.32$ cm spacing, we can achieve sensitivity better than 0.01 cm^3. This corresponds to less than 0.25% of the pore volume for the size of our core sample used in the displacement experiment.

Experimental Results

Saturations in static experiments: imaging and gravimetric comparison

First the validation of the average of the saturation distributions obtained using NMR images with the corresponding quantities obtained gravimetrically is considered using the Texas Cream limestone sample. Porosity and saturation distributions were obtained from multiecho profile images using the procedure reported previously (Chen et al., 1992). Figure 6 shows the saturation profile corresponding to various partial saturation states obtained using a centrifuge. For profile images of each saturation state, nonlinear regression was performed on a pixel-by-pixel basis using the multiexponential model. For each image, 15 pixels were randomly selected and the F-test was performed on these pixels. For all these pixels, the biexponential model was selected as the most suitable model. Saturations obtained by averaging the saturation distribution are compared to those by a gravimetric method as well as the average values calculated from distributions determined using other relaxation models. The average saturation values calculated with the biexponential model were within 4% of those obtained gravimetrically for the entire saturation range, while the other models yielded larger errors (up to 15%). This analysis validates the procedure for determination of saturation and emphasizes the role of model selection.

Determination of porosity distribution in the reservoir sandstone

Our previous dealing with fluid quantitation in porous media has been tested exclusively on cleaned outcrop sandstone and limestone samples. These outcrop rocks have little hydrocarbon deposits and contain relatively little paramagnetic impurities. Based on our measurements of more than 20 core samples, characteristic transverse relaxation times for those rocks range from about 5 ms in Berea sandstone to 16 ms in many carbonate rocks. In contrast, the T_2 values in many oil producing reservoir rocks may be much shorter due to higher levels of impurities. For four reservoir rock samples we have tested, the T_2 values are in the range of 1-3 ms with the low end corresponding to saturation with water and the upper end to saturation with refined oil. The T_2 difference between the outcrop and reservoir rocks may affect imaging acquisitions significantly since a typical NMR imaging apparatus requires a minimum waiting time (TE_{min}) greater than 2 ms for observation of images. During this time, a significant amount of the signal intensity will be lost if the sample T_2 is very short. Quantitation of images in porous media is further complicated by the fact that single-exponential relaxation decay is usually not observed. Sufficient data are required to select a suitable model that will provide accurate extrapolation to zero echo time.

The selected reservoir rock has a very short transverse relaxation time. The short component is about 2 ms (using the biexponential model) for most of the pixels even under fully oil-saturated conditions, and the average T_2 value under water-saturated conditions is only 1.3 ms. Figure 7 shows the T_2 relaxation decay data corresponding to complete water saturation for one single-image pixel. A total of 22 echoes were acquired with the TE times ranging from 2.3 to 30 ms. The three curves in the figure represent the nonlinear regression results using single, bi- and stretched exponential relaxation

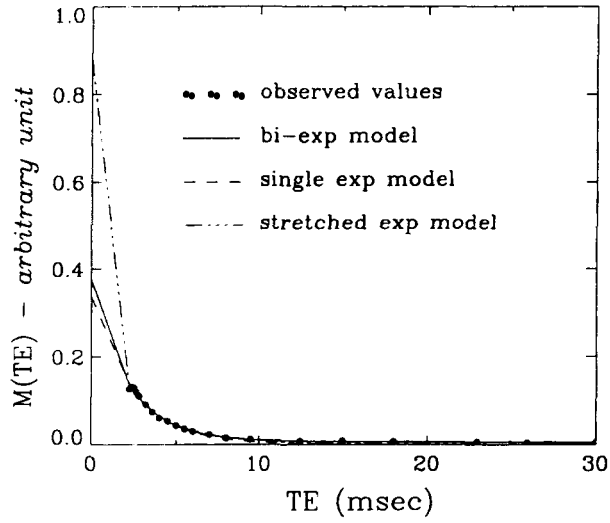

Figure 7. T_2 decay data and results of extrapolation using three models.

decay models, respectively. Comparing the experimental data and fitted biexponential curve shows that even at the smallest experimental echo time, the echo amplitude has already decayed to approximately one-third of its extrapolated value at $TE=0$. It is important to clarify whether the extrapolation method with the multiexponential model can still be used to successfully recover the significant contribution of the signal which has taken place before data are acquired. In our experiments, the images were acquired more frequently at short TE times than at longer TE times to avoid losing too much information regarding short components. This turned out to be necessary for the short relaxation times encountered in this sample.

The biexponential model was selected on the basis of the F-test. The porosity profile, calculated using that model, is shown in Figure 8. The average porosity calculated from the porosity profile is 20.1%, which is within 5% of the gravimetrically determined porosity (21.0%). While the small discrepancy may be due to experimental random error, it may also reflect the possibility that there is a very small component which may have been largely omitted by the biexponential model.

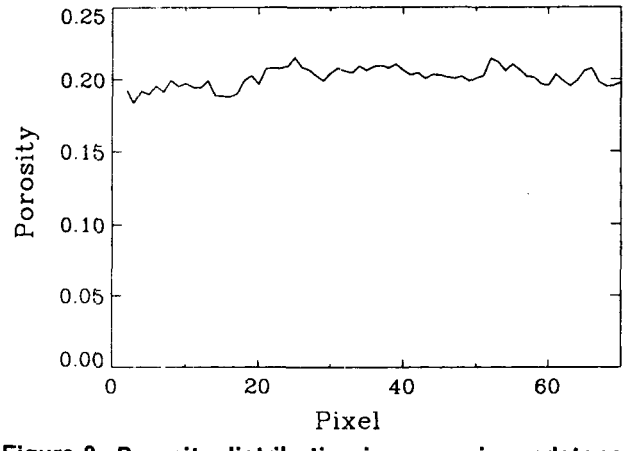

Figure 8. Porosity distribution in reservoir sandstone.

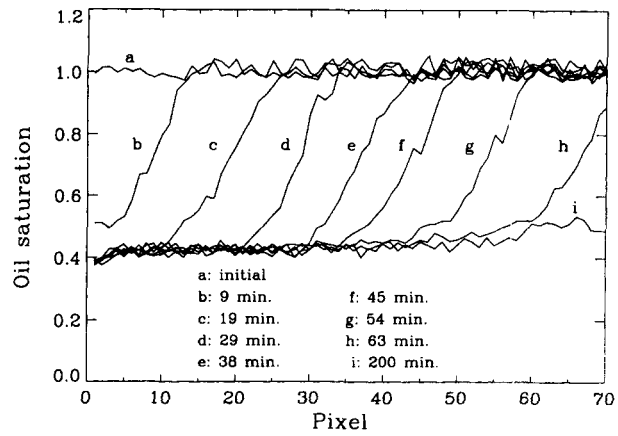

Figure 9. Saturation profiles obtained during imbibition in reservoir sandstone.

These results indicate that the procedure of using multiecho acquisition and multiexponential model for extrapolation can work very well in porous rocks, even for the very short T_2 cases, so long as the contributions of the short component(s) are not missed completely at the smallest imaging echo time. We conclude that this procedure is adequate at least for reservoir rocks with T_2 values on the order of 2 ms.

Figure 7 also shows that the stretched exponential relaxation function is not suitable for extrapolation for these very short T_2 rocks. Relaxation decay data for several pixels were analyzed using the stretched exponential model. The stretch exponent and intrinsic magnetization were determined using nonlinear regression. It was found that the echo amplitudes extrapolated to $TE=0$ for those pixels result in large errors. It is not surprising that such errors may occur using this model as the stretched exponential approximation is weighted toward the short time components. Considering that much information in the short TE region is not available in the imaging acquisition, the stretched exponential model may not be appropriate for the extrapolation in imaging of short T_2 reservoir rocks.

Saturation distributions in reservoir sandstone: imaging and dielectric measurements

Displacement experiments were also conducted in this reservoir sandstone. During the imbibition process, a slow flow rate (2 cm^3/h) was used to simulate the reservoir velocity. Figure 9 shows the oil saturation profiles during the displacement experiments. Each saturation profile was calculated from 22 different echo intensity profiles with 16 averages each. Since the T_1 relaxation time is also very short for this sample, fast repetition time ($TR=300$ ms) can be used so that the total imaging time was within 2 min. To reduce the possible systematic error due to flow artifacts during the image acquisition time, a random order of TE was used, even though moving artifacts were not expected to be significant under such a slow flow rate. The pixel size is $\Delta z=0.6$ mm. This corresponds to a $\Delta\nu_p$ of 1,320 Hz. Since the linewidth of this sample at $S=1$ is $\Delta\nu=2{,}000$ Hz, there would be certain overlap between the neighboring pixels for this susceptibility-limited resolution case. The oil-water interfacial front was clearly observed, even though the resolution may be somewhat affected by the large linewidth.

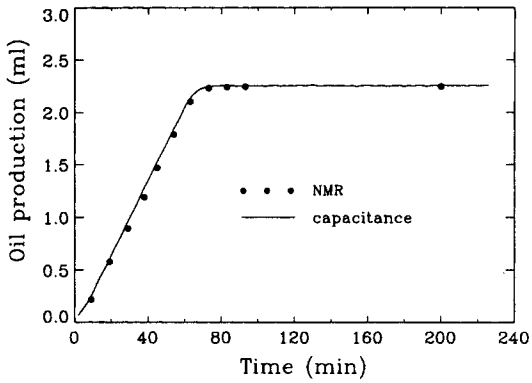

Figure 10. Oil production calculated by two methods.

The oil production was also determined during the displacement experiments using the electric capacitance measurements. Figure 10 plots the oil production evaluated using both the capacitance and imaging data. Qualitatively, the values calculated from the two methods match reasonably well. Some features of the comparisons are discussed below.

It is difficult to determine the time lapse between the start of flow experiments and the start of oil production reaching the capacitance device. This time lapse corresponds to the time required to allow produced fluids passing through the tubing between the outlet of the core and the capacitance device. In our experiment, the outlet tubing is initially filled with D_2O, the same fluid used for filling the capacitor initially. Therefore, the capacitance device will not show any sensitive change until this amount of D_2O has been completely pushed through the tube. Since this time delay will affect the production only for the capacitance measurements, but not for NMR images, the correction for the time delay effect is required when comparing productions obtained using the two methods. The data in Figure 10 have already taken into account the time delay. In the present case, the time delay was counted to be the time between the start of flow and the moment the capacitance meter starts to show noticeable change.

We are aware that the capability of accurate determination of this time lapse is critical for the production match between the data obtained using the two methods. This is particularly apparent for the data acquired before the displacing phase breakthrough. In Figure 10, we observed a little mismatch of the data obtained by the two methods in the time region before the breakthrough occurred. This mismatch can be attributed to the uncertainty in determining the exact time delay for capacitance measurement. If this is the correct reason, the mismatch corresponds to a time uncertainty on the order of 2 min. Nevertheless, the error percentage at any time during the displacement experiments never exceeded 5% of the total amount of oil corresponding to fully saturated state.

It is noted that a time lapse between the start of flow and the measuring of production is inevitable to all production measuring devices that require the accumulation of produced fluids. In this sense, image methods are inherently better since saturations of rocks are evaluated without time delay.

After breakthrough (at about 80 min), this discrepancy is less than 2% of the production but is slightly more than the fluctuating amplitude of capacitance measurements. The exact cause of this systematic error is still unknown. A possible cause may be due to a very small amount of oil initially in the inlet end tubing, which has been added to the oil saturation in the core region after the displacement experiment started. This amount of oil is eventually passed into the capacitor, thus increasing the amount of production.

Conclusions

It was demonstrated that NMR transverse relaxation time (T_2) and spectral linewidth ($\Delta\nu$) are saturation-dependent. These dependencies and their impact on imaging quantitation and resolution are critical. The procedure of using multiecho imaging acquisition and multiexponential relaxation extrapolation for fluid quantitation in porous rocks has been applied to analyze a reservoir rock that has very short transverse relaxation times. Satisfactory porosity and saturation measurements were obtained with this procedure. The averages of saturation distributions obtained by NMR imaging were validated using: (1) a gravimetric method in a limestone sample at various static partial saturation states and (2) dielectric (capacitance) measurements in a reservoir sandstone sample. In both cases, the saturation was satisfactory.

Acknowledgment

This project was supported in part by DOE Grant #DE-FG07-89BC14446. Financial assistance was also obtained from a University-Industry Cooperative Research Program for Petrophysical and Reservoir Engineering Applications of NMR at Texas A&M University, the State Land and Energy Resource Organization of Texas, and the Advanced Technology Program of Texas. The authors gratefully acknowledge input from Dr. C. M. Edwards during the initiation of research to use dielectric measurements for production measurements.

Notation

A_1 = surface area of plate occupied by water in capacitor
A_2 = surface area of plate occupied by oil in capacitor
C = capacitance
d = distance between two parallel plates
G = applied field gradient
k = calibration constant
l = height of plate in capacitor
m = $2N_c$
M = intensity of magnetization
M_0 = intrinsic intensity of magnetization
M^{cal} = calculated M
M^{obs} = observed M
n = number of observed data
n_p = number of pixels
N = linear proton density
N_c = number of components
N_i = linear density corresponding to $S = 1$
RSS = residual sum of squares
$RSS(N_c)$ = RSS using model with N_c components
S = water saturation
TE = echo time
TR = NMR pulse sequence repetition time
T_1 = longitudinal relaxation time
T_2 = transverse relaxation time

Greek letters

α = stretched exponent
γ = proton gyromagnetic ratio
$\Delta\nu$ = linewidth
$\Delta\nu_p$ = spectral width per pixel
$\Delta\omega$ = frequency domain width
Δz = length per pixel

ϵ_o = dielectric coefficient of oil
ϵ_w = dielectric coefficient of water
ρ = proton density in porous media
ϱ = proton density in fluid
ϕ = porosity
ω = angular frequency

Literature Cited

Edelstein, W. A., H. J. Vinegar, P. N. Tutunjian, P. B. Roemer, and O. M. Mueller, "NMR Imaging for Core Analysis," SPE paper #18272, Houston (Oct. 2-5, 1988).

Baldwin, B. A., and W. S. Yamanashi, "Detecting Fluid Movement and Isolation in Reservoir Cores Using Medical NMR Imaging Techniques," SPE paper #14884, p. 39 (1986).

Callaghan, P. T., *Principles of Magnetic Resonance Microscopy*, Clarendon Press, Oxford (1991).

Chen, S., F. Qin, K.-H. Kim, and A. T. Watson, "NMR Imaging of Multiphase Flow in Porous Media," *AIChE J.*, **39**(6), 925 (1993).

Chen, S., K.-H. Kim, F. Qin, and A. T. Watson, "Quantitative NMR Imaging of Multiphase Flow in Porous Media," *Mag. Reson. Imag.*, **10**(5), 815 (1992).

Hvollboll, H. T., "Method for Accurately Measuring Produced Oil Volumes During Laboratory Waterflood Tests at Reservoir Conditions," *Soc. Petro. Eng. J.*, **18**(4), 239 (1978).

Kerig, P. D., "Estimation of Relative Permeabilities from Displacement Experiments," PhD Diss., Texas A&M Univ. (1985).

Mandava, S. S., A. T. Watson, and C. M. Edwards, "NMR Imaging of Saturation during Immiscible Displacements," *AIChE J.*, **36**, 1680 (1990).

Potter, G. F., "Displacement, Saturation, and Porosity Profiles from Steady-State Permeability Measurements," SPE paper #19679, San Antonio (Oct. 8-11, 1989).

Sufi, A. H., H. J. Ramey, Jr., and W. E. Brigham, "Temperature Effects on Relative Permeabilities of Oil-Water Systems," SPE paper #11071, New Orleans (Sept. 26-29, 1982).

Weinbrandt, R. M., H. J. Ramey, and F. J. Casse, "The Effect of Temperature on Relative and Absolute Permeability of Sandstones," *Soc. Petro. Eng. J.*, **15**(5), 376 (1975).

Manuscript received May 12, 1993, and revision received July 12, 1993.